Garnet-Pyroxene Alteration Mapping in the Ludwig Skarn (Yerington, Nevada) with Geoscan Airborne Multispectral Data*

Abstract

Geoscan airborne multispectral image data of the skarn and calc-silicate-metamorphosed rocks near Ludwig (Yerington district, Nevada) have been analyzed and compared with published and unpublished maps. This study examines the spectral differentiation between two stages of garnet-pyroxene alteration, early metamorphic skarnoid and late metasomatic skarn. Both types of calc-silicate rock were successfully delineated using thermal infrared band difference images. Differentiation between the two alteration styles was achieved using a (0.717-μm − 0.873-μm) difference image, based on the deeper 0.87-μm Fe^{3+} garnet absorption in skarn.

Compositional variations, grain size, and weathering styles were examined as possible sources of this spectral variation. While all three contribute, weathering characteristics have the greatest effect. Skarnoid contains finer-grained and greater proportions of pyroxenes than skarn, which readily weather to a limonitic coat that mutes the 0.87-μm absorption.

Introduction

In their review paper on skarn deposits, Einaudi *et al.* (1981) describe skarn as "coarse-grained Ca-Fe-Mg-Mn silicates formed by replacement of carbonate-bearing rocks accompanying regional or contact metamorphism and metasomatism." The majority of the worlds tungsten is produced from skarn deposits and this deposit type is an important source of copper, iron, molybdenum, and zinc.

Despite their economic value, there is a distinct paucity of studies applying remote sensing to skarn deposits. The vast majority of remote sensing efforts in economic geology have been directed toward the identification of iron-staining or hydroxyl-bearing alteration products in porphyry copper or epithermal districts, or in the determination of regional structural trends. Skarns are a common feature in carbonate-bearing strata intruded by porphyry copper plutons (Einaudi, 1982) but, as Abrams and Brown (1985) comment in a study of the Silver Bell district, Arizona, "detection of most tactite (skarn) is unlikely because of the small size of outcrops and the lack of spectrally diagnostic minerals."

The increased spatial and spectral resolution of modern imaging spectrometers, however, suggests that such assertions be reevaluated. The Ludwig skarn in the Yerington district, Nevada, was selected for such a study. The geology of the area is well-characterized (Harris and Einaudi, 1982; Proffett and Dilles, 1984; Dilles and Einaudi, 1992), while extensive exposures and sparse vegetation cover provide ideal conditions for remote sensing. This study employs Geoscan AMSS Mk II image data and follows an approach similar to that of an exploration program:

- description of the setting and the target alteration types,
- selection of empirical image treatments based on spectral characteristics of the dominant minerals (acquired from both lab measurements of reconnaissance field samples and from the literature),
- comparison of the image processing results with geologic maps, and
- identification of the sources of spectral differentiation to determine whether the treatments can be exported to similar targets or are limited to the conditions present in the study area.

Instrumentation and Methods

The Geoscan AMSS Mk II scanner was first described by Lyon and Honey (1990). The AMSS Mk II was developed as a tool for mineral exploration by Geoscan Pty. Ltd., a division of Carr-Boyd Minerals based in Perth, West Australia. It is an imaging spectrometer using grating-dispersive optics with three sets of linear array detectors, one each in the visible/near infrared (VNIR), short-wave infrared (SWIR), and thermal infrared (TIR) (Table 1). The data set used in this study was flown 21 July 1990 (1250 PDT) at an elevation of 4700 ft above ground level (AGL), with a nominal pixel resolution of 3m.

Data acquisition by the Geoscan system differs from most other scanning systems in that the instrument gains and offsets are not fixed, but are adjusted for the conditions present along the flight line. The system is flown twice over the target area. During the first flight, an operator adjusts the gains and offsets in each channel to maximize the surface contrast into an 8-bit dynamic range (0 to 255). The same area is then flown a second time with the channels held constant at the new gains and offsets. By adjusting the offset values such that all channel means have a digital number (DN) of 127, the Geoscan data are effectively pre-corrected for the solar radiation curve (Rubin, 1991; 1993). This lessens the necessity for calibrations such as the "flat field" and log-residual (Green and Craig, 1985; Roberts *et al.*, 1986) in order to compare image data with reflectance. This method does require corrections for variation in the offset and gain settings (Windeler, 1992); raw Geoscan data were transformed to apparent reflectance using the "two-point correction"

*Presented at the Ninth Thematic Conference on Geologic Remote Sensing, Pasadena, California, 8-11 February 1993.

Photogrammetric Engineering & Remote Sensing,
Vol. 59, No. 8, August 1993, pp. 1277–1286.

0099-1112/93/5908–1277$03.00/0

Donald S. Windeler, Jr.
Department of Applied Earth Sciences, Stanford University,
Stanford, CA 94305.

TABLE 1. GEOSCAN CHANNEL WAVELENGTHS AND BANDWIDTHS (OCTOBER 1990 TO PRESENT)

	Band Number	Central wavelength (μm)	Bandwidth (μm)
	1	0.522	0.042
	2	0.583	0.067
	3	0.645	0.071
V	4	0.693	0.024
N	5	0.717	0.024
I	6	0.740	0.023
R	7	0.830	0.022
	8	0.873	0.022
	9	0.915	0.021
	10	0.955	0.020
	11	2.044	0.044
	12	2.088	0.044
S	13	2.136	0.044
W	14	2.176	0.044
I	15	2.220	0.044
R	16	2.264	0.044
	17	2.308	0.044
	18	2.352	0.044
	19	8.64	0.530
T	20	9.17	0.530
I	21	9.70	0.530
R	22	10.22	0.533
	23	10.75	0.533
	24	11.28	0.533

method of Lyon *et al.* (1975). Examples of transformed visible/near-infrared data are provided in the section on Image Data and Treatments. No thermal infrared spectrometer was available for this study, however, and thus uncalibrated thermal image data were used.

The data set exhibited considerable distortion perpendicular to the east-west flight direction, even after applying a panoramic correction. This distortion resulted from the combination of a relatively low flight level with considerable topographic relief (400-m increase from west to east on the image). The image data were registered to a 1:4800-scale topographic map using drainage junctions or other distinct geographic features as control points. The average RMS error between the registered image and the map is 7 to 8 pixels.

Color composite images in this study are described with a shorthand notation. The three single bands or band differences in an image are each given a subscript denoting their screen display color. For example, a "true color" treatment would be described as $(0.522\ \mu m)_B(0.583\ \mu m)_G(0.645\ \mu m)_R$ or, in Geoscan channels, $\mathbf{1}_B\ \mathbf{2}_G\ \mathbf{3}_R$.

Over 350 reflectance spectra were acquired from 202 samples collected by the author and 37 samples provided by M.T. Einaudi. Spectra were recorded from 0.4 to 2.5 μm using an IRIS Mark IV spectroradiometer manufactured by Geophysical Environmental Research, Inc. Halon was used as a reflectance standard.

Garnet and/or pyroxene compositions were analyzed by electron microprobe in 23 thin sections. These analyses were performed on a JEOL Superprobe 733 and calculated using ZAF corrections on a Kevex Sesame-Delta system. Typical operating conditions were 15-keV accelerating voltage, 20-nA beam current, 10-μm spot size, and 30-second count time. Albite was used as an Al and Si standard. Wollastonite and spessartine were standards for Ca and Mn, respectively, while oxides were used for Fe, Mg, and Ti.

Geology

Numerous workers have contributed to the understanding of the Yerington district, extending back to Knopf (1918). Regional studies have been conducted by Proffett (1977) and Proffett and Dilles (1984; in press). Information regarding the petrology and alteration of the Yerington batholith are provided by Dilles (1987) and Dilles and Einaudi (1992). Descriptions of skarn mineralogy and genesis in the district are summarized from Einaudi (1977), Harris (1979), and Harris and Einaudi (1982).

Triassic and Jurassic sedimentary and volcaniclastic rocks are exposed in the Singatse Range near Yerington, Nevada (Figure 1). These Mesozoic rocks were intruded and altered by a Jurassic quartz monzodioritic to granodioritic batholith. Early stage alteration of the Mesozoic rocks was largely metamorphic, resulting in the formation of fine-grained, garnet-pyroxene hornfels (skarnoid) in argillite, volcaniclastic, and silty limestone units. Skarnoid is iron-poor, with intermediate grossular-andradite garnets and diopsidic pyroxenes. Early stage alteration also formed garnet-pyroxene and plagioclase-idocrase-clinozoisite endoskarn in apophyses of quartz monzodiorite. Intrusion of granite porphyry dikes was accompanied by porphyry copper mineralization in the batholith and skarn formation in a massive limestone unit. Late stage skarn is metasomatic and iron-rich; garnets commonly approach pure andradite, and pyroxenes are salitic. Tertiary Basin and Range faulting has rotated the district ~90° westward, resulting in the horizontal exposure of a cross-section through the district as it was in Jurassic time (Proffett, 1977).

The textural, compositional, and genetic features of hornfels and skarn in the study area are summarized and compared in Table 2. From an exploration standpoint, the distinction between these two mineralogically similar alteration types can be critical; at Yerington, early hornfels altera-

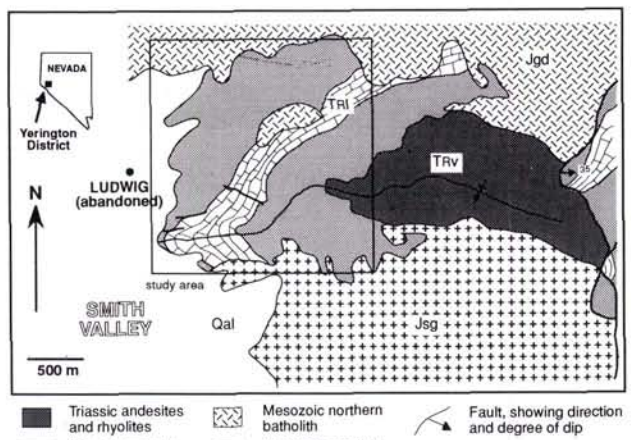

Figure 1. Generalized geologic map of the Ludwig area, Yerington district, Nevada (after Harris and Einaudi, 1982).

TABLE 2. COMPARISON BETWEEN SKARN AND HORNFELS (SKARNOID) ALTERATION TYPES IN THE LUDWIG STUDY AREA.

Hornfels	Skarn
• early, mostly metamorphic	• late, metasomatic
• extensively replaced silty limestone, calcareous argillite units; also replaced massive limestone and volcaniclastic units close to the igneous contact	• replaced massive limestone unit
• fine-grained (variable, most <0.5 mm)	• coarse-grained (0.1 to > 10 mm)
• iron poor garnets 40–60 mol % andradite pyroxenes < 15 mol % hedenbergite	• iron-rich garnets 65–100 mol % andradite pyroxenes 15–45 mol % hedenbergite
• barren, no associated mineralization	• mineralized, several small chalcopyrite orebodies

tion was barren, whereas skarn formation was locally accompanied by chalcopyrite mineralization.

Image Data and Treatments

Calc-Silicate Discrimination

The region of the electromagnetic spectrum between 8 and 13 μm is of particular interest to geologists because of the fundamental vibration of the Si-O tetrahedral bond. This vibrational absorption is a key feature in the spectra of the silicate rocks that make up much of the Earth's crust. The location of this absorption has been shown to shift to progressively longer wavelengths with depolymerization of SiO_4 tetrahedra and substitution of atomically heavier cations for Si (Lyon, 1962; 1965). This absorption shifts from 9 μm in felsic rocks (quartz, K-and Na-feldspar-rich) to nearly 12 μm in the most mafic rocks (Ca, Fe, Mg-rich) and thus can be an important tool for rock type identification.

Emittance spectra for quartz, feldspar, epidote, and grossular garnet are presented in Figure 2. The emittance minima for quartz and garnet are separated by more than 2 μm, a fortuitous occurrence that aids in discrimination between the two. In terms of Geoscan thermal bands, quartz and quartzofeldspathic rocks will be relatively dark in the 8.64-μm and 9.17-μm channels (**19** and **20**), whereas very mafic rocks will appear relatively dark in the 10.22-μm and 10.75-μm channels (**22** and **23**). In the case of the skarn body, a relative gradient between these channels (determined by either difference or ratio) should thus indicate quartz-rich (positive), calc-silicate (negative), or intermediate (flat) lithologies.

In order to discriminate between garnet-pyroxene-altered rocks and other lithologies, a thermal band difference treatment has been applied to the Ludwig 3-m data set in Plate 1a. This image displays $(10.75\text{-}\mu m - 9.70\text{-}\mu m)_B$ $(10.75\text{-}\mu m - 9.17\text{-}\mu m)_G$ $(10.75\text{-}\mu m - 8.64\text{-}\mu m)_R$ and has been smoothed using a 3 by 3 low pass filter to eliminate excess noise. In this orientation, north is to the right and the top of the image corresponds to exposures closer to the paleosurface. Garnet-pyroxene rock appears dark, while quartz and feldspar-rich material is bright. This treatment also identifies the drainages which carry alluvial skarn and hornfels. Hereafter, this difference treatment will be referred to by its Geoscan channels: $(\mathbf{23\text{-}21})_B(\mathbf{23\text{-}20})_G(\mathbf{23\text{-}19})_R$.

A distribution map of garnet-pyroxene rock is presented in Plate 1b. Comparison between the $(\mathbf{23\text{-}21})_B(\mathbf{23\text{-}20})_G(\mathbf{23\text{-}19})_R$ image and the geologic map shows an extraordinary correlation. It is apparent that the overall distribution and morphology of garnet-pyroxene skarn and hornfels are clearly defined by the thermal differences treatment. Several common points of reference are indicated by numbers 1 to 5 on Plates 1a and 1b; other features of note or mismatch are indicated on the image with smaller numbers. All annotated features are briefly described in Table 3.

Epidote also appears dark on this treatment because of its long-wavelength absorptions between 10.5 and 11 μm (Salisbury *et al.*, 1991). This is most apparent near the southern edge of the image (area 6), where several dark anomalies not identified on the garnet-pyroxene map result from exposures of andesite altered to massive epidote.

Bright responses on the $(\mathbf{23\text{-}21})_B(\mathbf{23\text{-}20})_G(\mathbf{23\text{-}19})_R$ image correspond to quartz- and feldspar-rich lithologies. The lone bright yellow spot on the northwest edge is a quartzite (area 7), while the north-northeast-trending white area immediately west of the main exposures of garnet-pyroxene rock results from a felsite unit (area 8). The bright area on the eastern edge is a tightly folded rhyolite flow (area 9).

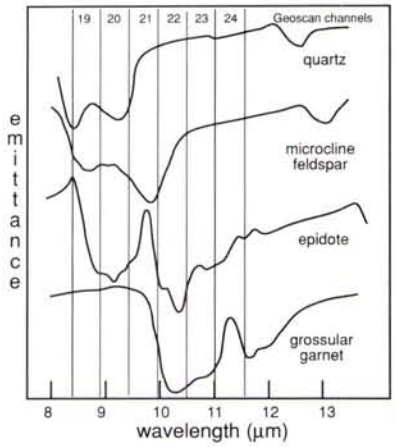

Figure 2. Emittance spectra of quartz, feldspar, epidote, and grossular garnet. The quartz, feldspar, and grossular garnet spectra are direct emittance measurements from Lyon and Green (1975). The epidote spectrum is calculated from a reflectance measurement from Salisbury *et al.* (1991; sample Epidote.1, fracture surface) using Kirchoffs Law (E = 1-R).

TABLE 3. COMMON REFERENCE POINTS FOR PLATES 1A AND 1B (NOS. 1 TO 5) AND ADDITIONAL AREAS OF INTEREST OR DISAGREEMENT ON THE IMAGE DATA (NOS. 6 TO 11).

	Image-map reference points
1	Douglas Hill Mine
2	west and south outcrops of the Casting Copper mine
3	Greenwood Breccia
4	Garnet Hill
5	major drainage carrying alluvial garnetite
	Other features of note
6	massive epidote alteration; dark on image because epidote absorption in ch. **22** & **23** is similar to garnet (see Fig. 2.)
7	quartzite; yellow on image because of quartz absorption in ch. **19** & **20**
8	"felsite" (f.g. quartz-feldpar rock); white on image because of quartz and feldspar absorptions in channels **19** through **21**
9	rhyolite; same comments as felsite
10	gypsum; orange to red on image because of gypsum absorption in ch. **19** (±**20**)
11	alluvial garnetite deposit; may be erosional remnant from Basin and Range faulting (M.T. Einaudi, pers. comment)

Gypsum dumps in the northwest (area 10) appear red to orange on the $(\mathbf{23\text{-}21})_B(\mathbf{23\text{-}20})_G(\mathbf{23\text{-}19})_R$ treatment. This was not initially expected but follows from the thermal spectrum of gypsum. The sulfate ion has intense absorptions at 8.3 and 8.7 μm which are narrow relative to the Si-O absorption in quartz (Lyon, 1964). This absorption would appear in the 8.64-μm and (to a lesser degree) 9.17-μm channels (**19** and **20**), and is thus brightest on the (**23-19**) difference (red on this treatment).

Skarn/Hornfels Discrimination

VISIBLE/NEAR-INFRARED SPECTRAL FEATURES OF GARNET-PYROXENE SKARN AND HORNFELS

Thermal difference images were effective at defining areas of calc-silicate alteration in the study area, but could not differentiate between skarn and hornfels. The VNIR laboratory spectra of skarn and hornfels samples from Yerington were compared in order to identify features that could be used for discrimination. Garnet and pyroxene comprise the dominant mineralogy of these alteration types and generally determine the spectral features. Garnets in the study area fall within the grossular ($Ca_3Al_2Si_3O_{12}$) - andradite ($Ca_3Fe_2Si_3O_{12}$) series (Harris, 1979). With these compositions, the spectra of Yerington garnets are dominated by effects of Fe^{3+} in the octahedral site. The reflectance spectra of andradite-grossular garnets show two major Fe features: a strong drop in reflectance toward the UV due to charge transfer and a crystal field reflectance minimum at 0.87 μm (Hunt *et al.*, 1973).

The visible and near-infrared spectral features of pyroxenes have been studied in much greater detail than those of the garnets, due to their probable importance in the remote sensing of planetary surfaces. A paper by Straub *et al.* (1991) contains a concise discussion of the theory behind and interpretation of pyroxene spectra in their investigation of the spectral effects resulting from pyroxene oxidation, as well as additional references. The following discussion has been summarized from the latter paper.

Pyroxenes have a structural formula of $(M1)(M2)Si_2O_6$. Metal cations occur in two crystallographic positions, the M1 and M2 sites. Pyroxenes in the Ludwig area are calcic clinopyroxenes of the diopside ($CaMgSi_2O_6$)-hedenbergite ($CaFeSi_2O_6$) series (Harris, 1979). In calcic clinopyroxenes, Fe^{2+} and Mg^{2+} occupy the M1 position and Ca^{2+} fills the M2 site. Spectra are dominated by Fe^{2+} absorptions near 0.95 and 1.15 μm. While these are weaker than absorptions caused by Fe^{2+} in the M2 site (e.g., pyroxenes of the enstatite-orthoferrosilite series, $(Fe, Mg)SiO_3$), the greater crystal field stabilization energy imparted to the Fe^{2+} ion in clinopyroxenes results in absorptions that are considerably stronger than the Fe^{3+} bands present in garnets.

Bidirectional reflectance spectra of three skarn samples and four hornfels samples are presented in Figures 3a and 3b, respectively. The three skarn samples (YER3-5, YER3-33, and YER4-4) display progressively increasing garnet:pyroxene ratios. The hornfels samples (Figure 3b) are also arranged in order of decreasing pyroxene content from YER6-19 to MTE 502 and 514 to MTE 305.

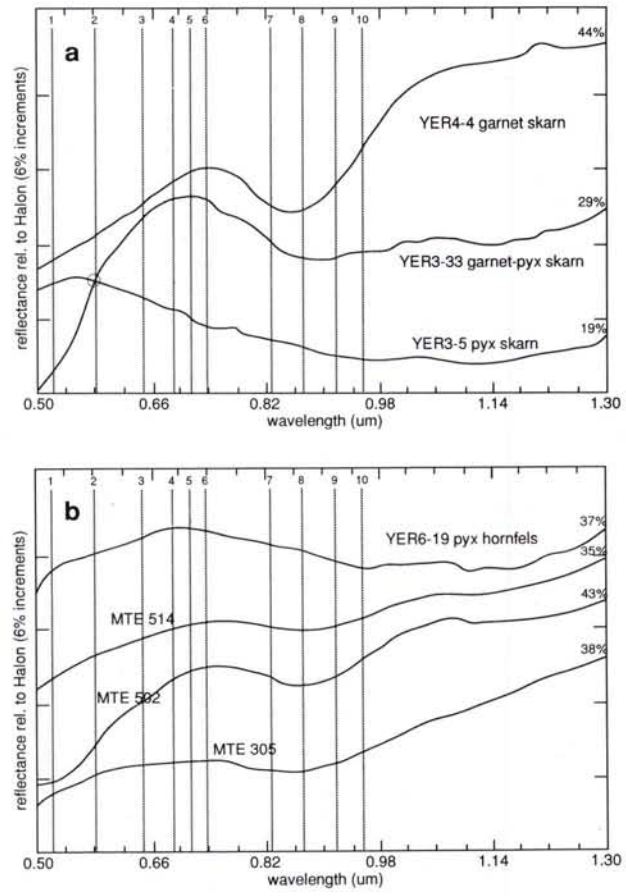

Figure 3. Bidirectional reflectance spectra of garnet-pyroxene (a) skarn and (b) hornfels samples. Spectra have been offset for clarity; actual reflectance at 1.3 μm is labeled. Geoscan band centers are included.

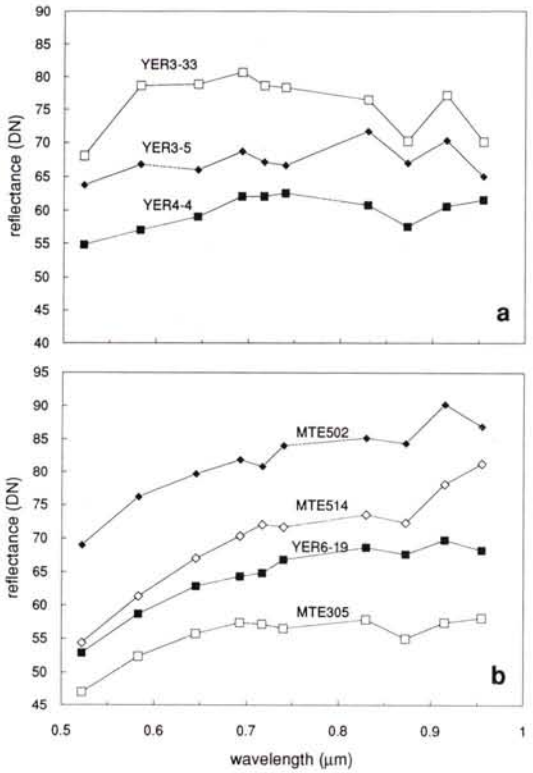

Figure 4. Corrected Geoscan spectra extracted from image for samples used in Figure 3. Data are averages of four pixels. Some curves have been slightly offset (< 5 DN) for clarity.

Pyroxene-rich sample YER3-5 shows a strong, broad absorption centered near 1.1 μm, resulting from Fe^{2+} in pyroxene M1 sites. The reflectance maximum at 0.55 μm is not directly related to an electronic transition but is a "window" between two strong absorptions, the M1 crystal field at 1.1 μm and the intense Fe-O charge transfer in the UV. Sample YER3-33 (garnet-pyroxene ratio 60:40) still shows a weak pyroxene band at 1.1 μm, but the spectrum is now dominated by ferric absorption through 0.55 μm and at 0.87 μm. Sample YER4-4 is nearly pure andradite garnet, and the spectrum shows a well-developed 0.87 μm ferric band.

Sample YER6-19 (Figure 3b) is a pale green, fine-grained diopside hornfels with significant (20 to 30 percent) garnet. The spectrum exhibits two Fe^{2+} absorptions: a weak 0.95-μm and an asymmetric 1.1-μm feature. Sample MTE 514 consists of 80 to 90 percent isotropic garnet, with the remainder fine-grained pyroxene needles; the VNIR spectrum shows the 0.87-μm garnet absorption and a weak 1.2-μm band of indeterminate origin. Sample MTE 502 also consists of 80 to 90 percent isotropic garnet (0.2- to 1.0-mm diameter) with intimately intergrown pyroxene and epidote. The spectrum is nearly identical to that of MTE 514 but shows a slightly stronger 0.87-μm garnet absorption and a steeper slope toward the blue and UV. This is probably an effect of the protolith, a dolomitic marble. Hornfelses and skarn formed in pure carbonate tend to contain fewer precursor mineral inclusions and typically show stronger spectral features as a result. Sample MTE 305 formed in silty limestone and contains 80 to 85 percent anisotropic garnet with semi-opaque inclusions as the remainder. Only the garnet band at 0.87 μm is present in the VNIR.

The majority of the skarn and skarnoid in the study area are garnetites containing lesser, varying quantities (0 to 20 percent) of pyroxene. In spite of the much stronger spectral features of pyroxene, the spatial prevalence of garnet-rich rocks results in most skarn and hornfels spectra being dominated by the ferric iron garnet signature. In laboratory spectra measured from reconnaissance field samples, skarn tended to show a deeper 0.87-μm minimum than did hornfelses. This suggested that Geoscan channel **8** (0.873 μm) might be used to discriminate these alteration products.

In order to determine whether this difference in absorption depth was also present in the Geoscan data, pixel spectra were extracted from the image locations of these same seven samples (Figures 4a and 4b). These spectra are not strictly comparable with those in Figures 3a and 3b, as these laboratory spectra were measured from fresh surfaces and the image data represent weathered material. Nevertheless, the skarn samples in Figure 4a show a deeper local minimum in channel **8** than the hornfels samples in Figure 4b.

Skarn/Hornfels Image Treatments and Results

The treatment that proved most useful at differentiating between skarn and hornfels applied a (0.717-μm − 0.873-μm) band difference (Geoscan channels **5-8**). The bright areas on the smoothed (**5-8**) single band image of the study area (Plate 2a) match well with the mapped distribution of skarn (Plate 2b). Only a few DN separate these anomalies from background, however; contrast stretching was used to identify areas that were obviously brighter than the norm.

A number of areas not mapped as skarn appear bright on this treatment and are annotated on Plate 2a. Several are small garnetite dumps from the Douglas Hill mine (1). Muscovite schists and pyritic hornfels in the andesite unit immediately east of the main skarn body (2) are heavily stained with iron oxides; limonite (goethite?) is the dominant mineral, but hematite is common and jarosite locally is present along fractures. The outcrop and dumps of the Ludwig silica-pyrite body (3) are similarly iron-stained, but hematite is less common and no jarosite was observed. These iron minerals show a strong crystal field absorption ranging from 0.87 μm (hematite) to 0.95 μm (goethite), just as do garnets containing ferric iron (Townsend, 1987). Strongly iron-stained rocks give a (**5-8**) value similar to that of garnet skarn, particularly if hematite is present.

Possible Sources of Skarn/Hornfels Discrimination

The observed spectral discrimination between the garnet-pyroxene skarn and garnet-pyroxene hornfelses could result from differences in composition, grain size, weathering styles, or any combination of the three. Garnets and pyroxenes in skarn are considerably more iron-rich than those in skarnoid; given that the (0.717-μm − 0.873-μm) treatment used above takes advantage of the 0.87-μm Fe^{3+} absorption in garnet, the higher (**5-8**) values in skarn may result from the higher iron content. It is well established that depth of an absorption feature increases with increasing grain size (Adams and Filice, 1967; Clark and Roush, 1984), a factor which would also favor a deeper absorption feature in the coarser-grained skarn. Weathering may affect skarn and hornfels differently and should be considered a critical factor in any study concerned with spectral differentiation.

Laboratory spectra were averaged over Geoscan band-passes for comparison with the airborne data. When analyzing laboratory spectra, ratios of reflectance are often

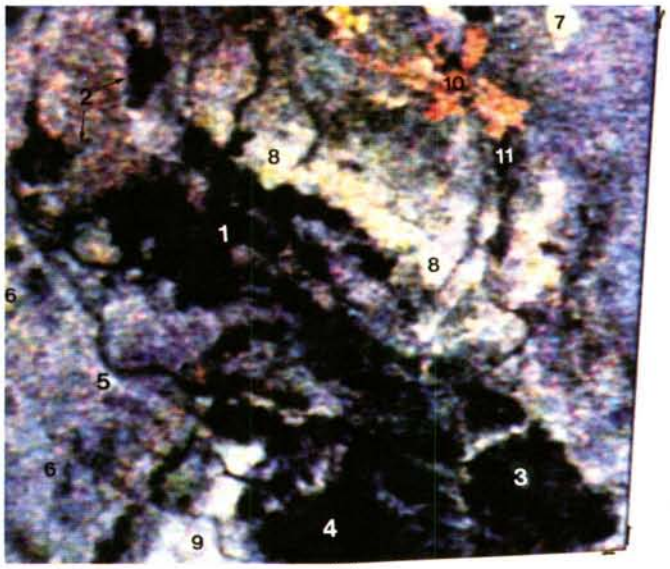

(a)

(a)

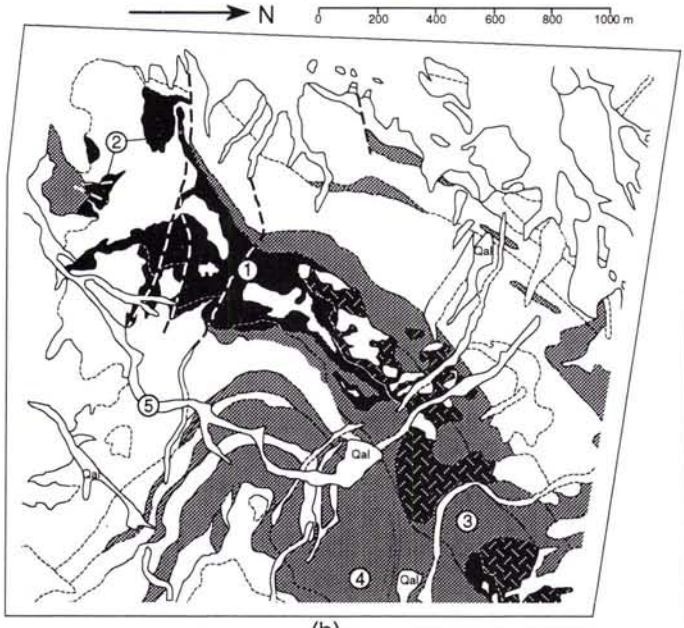

(b)

Plate 1. (a) Geoscan (**23-21**)$_B$(**23-20**)$_G$(**23-19**)$_R$ color composite calc-silicate treatment. Garnet-pyroxene and epidote rocks appear black on this treatment. (white/yellow = quartz and feldspar-rich rocks, orange/red = gypsum). This image covers an area 2.1 km from left to right, with north to the right. (b) Distribution of garnet-pyroxene rock in the Ludwig area. (grey = skarnoid, black = skarn, black patterned = endoskarn.) From Harris (1979), Einaudi (unpub.).

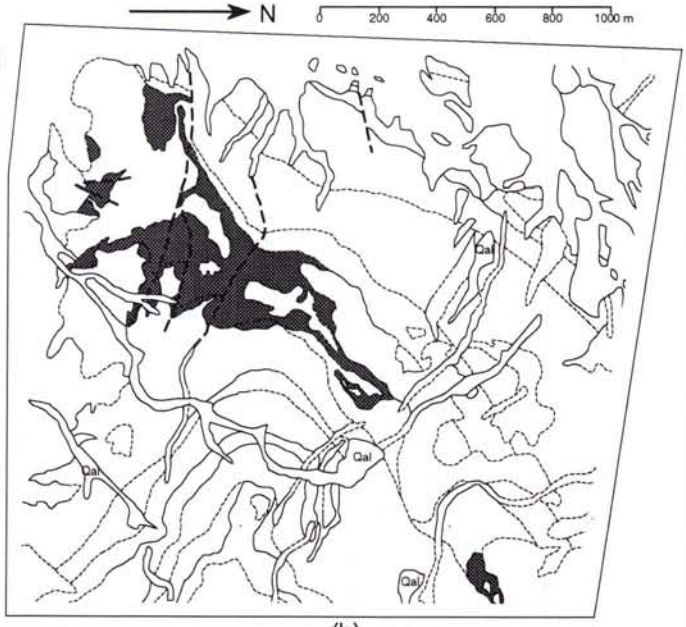

(b)

Plate 2. (a) Geoscan (**5-8**) skarn/hornfels discriminator treatment. Bright areas are garnet-pyroxene skarn and strongly Fe-stained rocks. This image covers an area 2.1 km from left to right, with north to the right. (b) Distribution of skarn rock in the Ludwig area. From Harris (1979).

employed to isolate the relative absorption strength (Clark and Roush, 1984). In this study, differences were used in order to duplicate the conditions of the image treatments. All difference analyses were checked with ratios, however, and in no cases were there significant effects on the results.

Compositional Effects

The 0.87-μm absorption feature results from Fe^{3+} within a mineral or in a weathering coat on the surface of a mineral. Given the dichotomy in iron content between Fe-rich skarn and Fe-poor hornfels, compositional variations must be con-

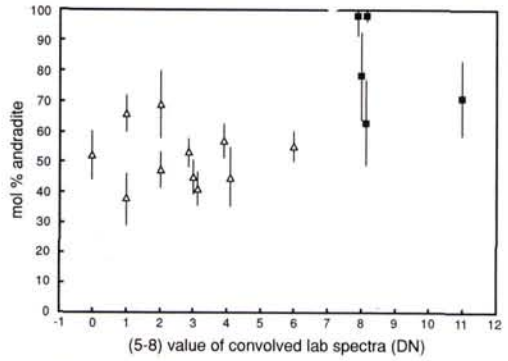

Figure 5. Plot of molar percent Fe-endmember composition of garnets vs. (**5-8**) values. The (**5-8**) values are calculated from laboratory spectra (0 to 100 percent) averaged over Geoscan bandpasses and multiplied by 2.55 to allow comparison with the 8-bit (0 to 255) Geoscan data. Bars represent one standard deviation. Open triangles represent hornfels, closed squares are skarn.

sidered as a possible source for the observed spectral discrimination. If the depth of the absorption feature increases with Fe content, it would fit the observed pattern of larger (**5-8**) values in skarn.

There is some empirical support for such a hypothesis. Moore and White (1972) studied the absorption spectra of nine garnets in the andradite-grossular-uvarovite series as a function of their composition. They found a linear relationship between absorbance and weight percent Fe_2O_3 for five absorption bands between 0.35 and 0.75 μm. However, several factors prevent the direct application of their results to this study. Moore and White (1972) did not examine the 0.87-μm absorption band of interest in the Yerington garnets. They studied only shorter wavelength bands, none of which could be resolved in reflectance spectra of garnets used in this study. Their samples contained no garnets with intermediate compositions similar to those found in the Yerington hornfels; their grossularitic samples had compositions ranging from ad_8 to ad_{26}, while their andraditic samples had compositions of ad_{93} and ad_{94}. Finally, they found absorbance to be a linear function of Fe_2O_3 content; reflectance, however, does not vary directly with absorbance and would not necessarily show a linear relationship. Nonetheless, their study lends credence to the hypothesis that the 0.87-μm absorption feature would deepen with increasing Fe.

To test this hypothesis, reflectance spectra averaged over Geoscan bandpasses were compared to composition for 16 garnet- pyroxene skarn and hornfels samples in the study area. All samples consist of >70 percent garnet. Samples were selected that minimized spectral effects not related to garnet composition; all are free of opaques or inclusions and showed little or no alteration to epidote or other secondary minerals. Figure 5 shows the (**5-8**) values of convolved laboratory spectra versus the average molar percent Fe-endmember of garnets as determined by electron microprobe.

There is a definite trend toward an increasing (**5-8**) value with mole percent andradite shown in Figure 5. Two comments with respect to the spectra used in this plot should be noted, however. These laboratory spectra were measured from cut surfaces, a precaution to reduce possible shadowing effects. If garnetite exhibited a tendency to fracture along rims of a given composition, a cut surface would not yield a spectrum representative of the "typical" garnetite hand sample. No such tendencies have been noted in this study area, but the possibility should not be disregarded in similar studies. More importantly, these are spectra of hand samples and the effects of grain size have not been removed. This factor is considered in the following section. While these caveats suggest that this relation may not be applicable to all skarn deposits, the data presented in Figure 5 indicate that the majority of the garnetiferous rocks at Yerington exhibit a trend toward stronger 0.87-μm absorption with increasing iron content.

Grain Size/Textural Effects

In a study of the reflectance characteristics of olivines as a function of composition, King and Ridley (1987) found systematic spectral variations with Fe/Mg ratios and with Ni impurities but cautioned:

> "The area of an absorption band, i.e., the area under a straight-line continuum, is not simply related to the Fe/Mg ratio of the sample unless the grain size is severely restricted ... . The area of the 1-μm absorption band is positively correlated with grain size fractions of a given olivine composition." (p. 11,468.)

It is well established that the spectrum of a particulate material is strongly affected by its grain size (Adams and Filice, 1967; Clark and Roush, 1984). As grain size decreases, overall brightness increases and spectral features become less pronounced. The skarns in the study area definitely tend to be coarser grained than the skarnoid; an increase in the depth of the 0.87-μm feature with grain size could result in the larger (**5-8**) values for skarn.

Unfortunately, a comparison between grain size (estimated from thin section) and (**5-8**) value for 22 samples proved inconclusive. The data suggested that the depth of the 0.87-μm absorption increased with depth, but with a correlation coefficient of only 0.26. The strongest evidence for the importance of grain size effects on spectra lies in their identification in numerous other studies (Adams and Filice, 1967; Clark and Roush, 1984; Crowley, 1986; King and Ridley, 1987; Windeler and Lyon, 1991).

A common feature in the hornfelses is the occurrence of many fine-grained mineral inclusions in garnet; such samples were excluded from the comparison because the presence of numerous inclusions would make the estimation of the "average" grain size difficult. However, this is a textural effect that would effectively result in a finer grain size. Alternatively, mineral inclusions can be opaque materials that absorb across all wavelengths. Mineral inclusions in garnet are much more common in the hornfelses than in skarn and are yet another effect that would favor deeper spectral absorption features in skarn.

Weathering Effects

The rocks of the Yerington district are not deeply weathered. Outcrops are plentiful and most hilltops and hillsides lacking outcrops are covered with a surficial layer of residual rock fragments (desert pavement) reflecting the underlying lithology.

Nonetheless, electromagnetic radiation in the visible and short wave infrared regions is most strongly affected by the top 50 μm of a surface and is thus highly sensitive to weathering (Buckingham and Sommer, 1983). Figure 6 illustrates the importance of weathering on spectral features. The mean (**5-8**) values for laboratory spectra of skarn and hornfels samples averaged over Geoscan bandpasses were compared.

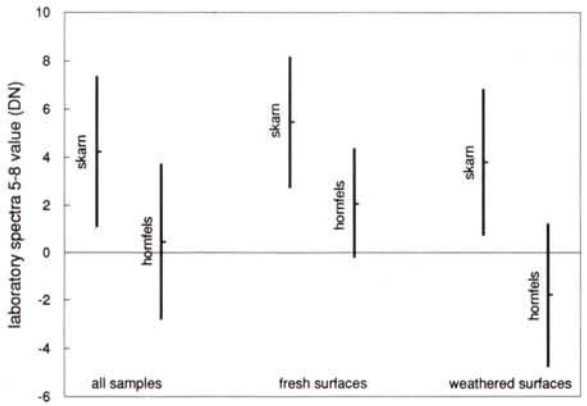

Figure 6. Average (**5-8**) values for convolved laboratory spectra of skarn and hornfels, fresh and weathered. Horizontal ticks are means, vertical bars represent one standard deviation.

While the (**5-8**) values for skarn tend to be higher than those for hornfels, there is significant overlap. When the data are subdivided into spectra of fresh (broken surfaces, thin section heels) and weathered samples, however, the sets of weathered skarn and hornfels are distinctly more separable than the fresh.

In order to lessen possible sampling errors in this analysis, (**5-8**) values were compared for spectra of fresh and weathered surfaces of 28 samples (Figure 7). Weathering reduced the (**5-8**) value for all skarnoid samples examined, while for skarn samples weathering resulted in little or no change. In five samples (denoted by a dotted connecting line) weathering actually increased the (**5-8**) value in the skarn. The skarn sample with the greatest drop in (**5-8**) value, YER7-44, is weakly coated with desert varnish and thus probably does not represent a typical fresh/weathered pair of spectra. The spectral differentiation between skarn and hornfels clearly is due in part to differences in their weathering characteristics.

The weathering characteristics of the garnet-pyroxene rocks in the study area vary with texture and mineralogy. As pyroxenes weather much more readily than garnets, their weathering properties would have a more immediate effect than those of the garnets. Fine-grained rocks develop surface coatings more readily than coarse-grained rocks. Garnet-pyroxene hornfelses in the study area typically weather to a brown or dark red-brown color suggestive of goethite. Fine-grained pyroxene skarn acquires a similar brown (goethitic) or reddish-brown (hematitic) coat, whereas coarse, bladed salite is coated locally but tends to retain the grey-green color of the fresh pyroxene. Garnet-dominated skarn shows fewer surface weathering effects than the finer-grained skarnoid; the weathered surfaces of garnet-pyroxene skarn darken slightly, while garnet skarn exhibits little color change and the glassy luster of the fresh garnets usually is preserved. Overall, the garnet-pyroxene hornfelses contain greater proportions of finer-grained pyroxene than skarn. The better-developed limonitic coats on skarnoid undoubtedly result from this abundance of readily-weathered, fine-grained pyroxenes.

Most calc-silicate altered rocks in the Ludwig area consist predominantly of garnet but contain significant pyroxene. For these garnet-rich rocks, spectra of weathered surfaces differ from fresh surfaces in the VNIR in several ways (Figures 8a and 8b):

(1) The average albedo decreases;
(2) The slope of the spectrum at wavelengths shorter than 0.7 μm may steepen; and
(3) The Fe^{3+} absorption feature resulting from garnet is usually retained, but is often canted downward towards the shorter wavelengths as a result of (2) While this results in an apparent shift of the band location, isolation of the absorption feature by continuum removal proves this to be an illusory effect (Clark and Roush, 1984).

Whereas the garnet-rich rocks absorb strongly in the UV and thus also have relatively steep positive slopes into the visible, fine-grained iron oxides exhibit a steeper slope because of their "trans-opaque" behavior. At the longer wavelengths, reflectance increases with decreasing grain size (trans-), while at shorter wavelengths absorbance increases with decreasing grain size (-opaque). The slope break between these two regions occurs near 0.55 μm (Salisbury and Hunt, 1968).

The spectra of pyroxene-rich rocks (Figure 8c) change similarly on weathering, although they differ from those of the weathered garnets due to differences in the original sample spectrum. Sample albedo decreases with weathering at wavelengths shorter than 0.6 μm but increases at longer wavelengths, again due to the trans-opaque behavior of the oxides. A study by Straub *et al.* (1991) determined that on oxidation of Fe^{2+} in calcic clinopyroxenes to Fe^{3+}, the Fe^{2+}-Fe^{3+} charge transfer transition (0.75 μm) masked the Fe^{2+} crystal field absorption feature. They also found evidence for nanophase (particle diameters <10 nm) hematite on oxidized surfaces. In this study, the strong, broad 0.95- and 1.1-μm Fe^{2+} absorption bands in the pyroxenes remain but are typically less well-defined than on fresh surfaces. An absorption may develop near 0.9 μm but is typically broad and shallow.

Effects (2) and (3) thus give a possible justification for the drop in (**5-8**) values between fresh and weathered hornfels samples illustrated in Figures 6 and 7. Fine-grained pyroxenes weather to iron oxides, and the spectral qualities of this oxide coat reduce the continuum reflectance in channel **5**. The strongest effects of the limonite coat are seen in the visible region; channel **8** is less affected or unchanged by this coating and thus the (**5-8**) value decreases. As the inten-

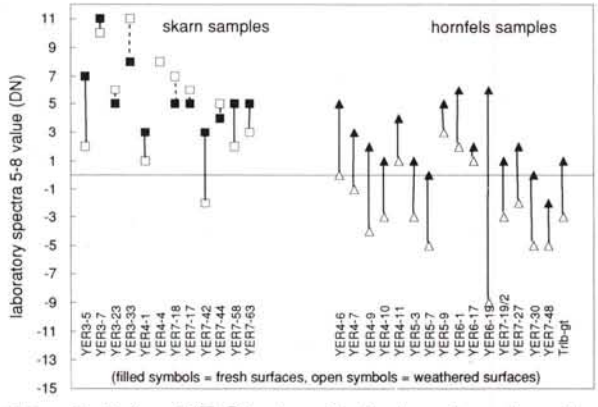

Figure 7. Pairs of (**5-8**) values for fresh and weathered surfaces of 12 skarn and 16 hornfels samples. Open symbols represent fresh surfaces, closed are weathered. Solid connecting lines indicate a decrease in (**5-8**) on weathering, dotted lines indicate an increase.

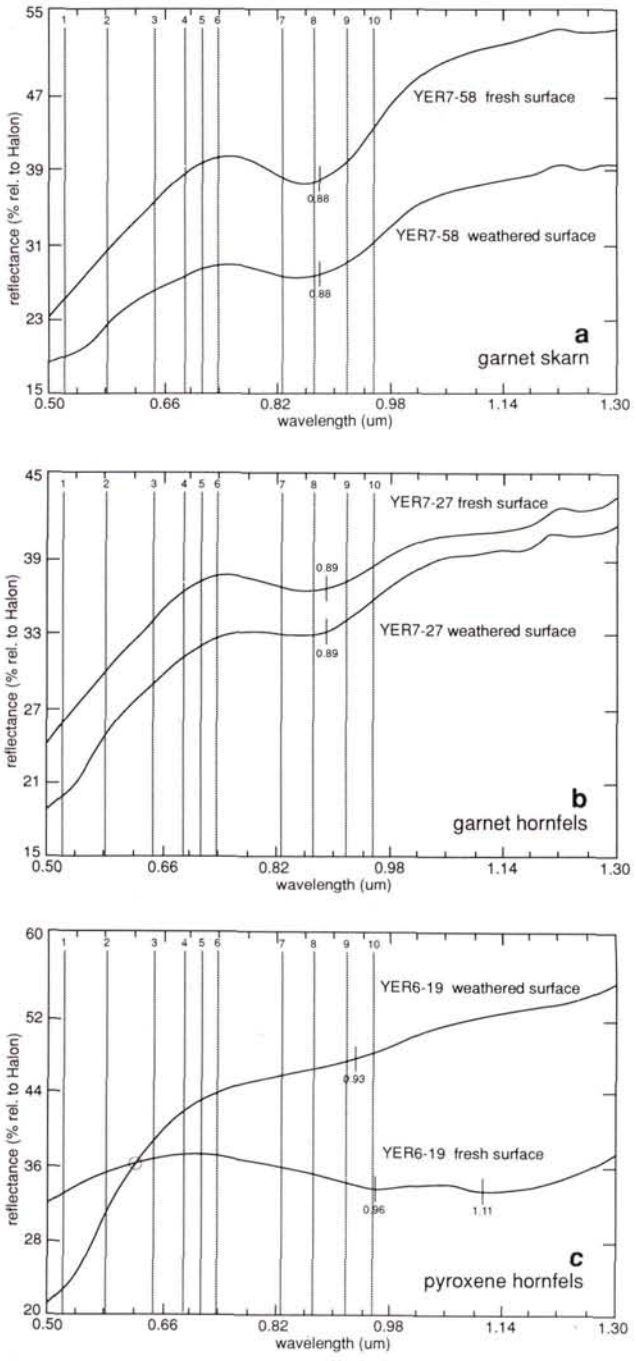

Figure 8. Reflectance spectra of fresh and weathered surfaces of (a) garnet skarn, (b) garnet hornfels, and (c) pyroxene hornfels samples. Vertical ticks give locations of reflectance minima after hull (continuum) removal. Curve crossovers are circled. Geoscan band centers are included.

sity of the iron-oxide staining increases, however, the ferric iron absorption near 0.86 (hematite) or 0.93 μm (goethite) deepens with a concomitant increase in the (**5-8**) value; this would explain the (**5-8**) anomaly in Plate 2a for the heavily goethite- and hematite-stained andesites and for the goethitic gossans of the Ludwig silica-pyrite body.

Conclusions

Thermal IR difference images were successful in defining the distribution of garnet-pyroxene skarn and hornfels in the Ludwig study area, while a (0.717-μm − 0.873-μm; **5-8**) difference image provided a means of differentiating between the two. Areas heavily stained by iron oxides were present as errors of inclusion on the (**5-8**) image, but the additional information gained through the thermal IR differences could readily be included to distinguish these from skarn. One simple method would be a $(\mathbf{23\text{-}20})_B(\mathbf{5\text{-}8})_G(\mathbf{23\text{-}19})_R$ image (Windeler, 1992). Alternatively, this combination of thermal and VNIR band differences could be used as a means of identifying iron-stained, silicified rocks - common targets in mineral exploration.

Compositional, grain size, and weathering variations were investigated as possible sources for the skarn/hornfels discrimination displayed by the (0.717-μm − 0.873-μm; **5-8**) difference image. All three factors contribute, but spectral variations due to weathering appear to be the most important. These results are summarized in Table 4.

Skarn/hornfels discrimination in the Yerington contact aureole thus appears to result from several spectral variations that fortuitously all contribute in the same direction. Whether this treatment would be effective in other districts is uncertain, although higher iron contents and coarser grain size relative to early hornfels are common features of skarn districts (Einaudi *et al.*, 1981). The VNIR spectral effects of manganese may also play a role, particularly in Pb-Zn skarns. However, the use of multispectral thermal infrared data for detection of garnetiferous rocks should be generally applicable to skarn exploration. Most skarns are associated with felsic to intermediate intrusions, which would have emission spectra distinct from the relatively long-wavelength minima of garnetites in the 8- to 13-μm region. Discrimination between different stages of calc-silicate alteration may often depend on site-specific, empirically determined treatments.

Acknowledgments

The author would like to thank his thesis advisors, Ron Lyon and Marco Einaudi, for all the help and constructive criticism offered throughout the duration of this research. Credit for the alteration mapping also belongs to Marco for unpublished work done with the Anaconda Company in the 1970s. I would also like to thank Frank Honey and Geascan Pty. Ltd. for providing the imagery of the Ludwigskarn. Reviews by Stuart Marsh and Veronique Carrere helped to improve the manuscript and a question at ERIM by Roger Clark identified a blind spot that needed to be checked out.

References

Abrams, M. J., and D. Brown, 1985. Silver Bell, Arizona, porphyry copper test site report, *The Joint NASA/Geosat Test Case Project,* American Association of Petroleum Geologists, Tulsa, pp. 4.1–4.73.

Adams, J. B., and A. L. Filice, 1967. Spectral reflectance 0.4 to 2.0 microns of silicate rock powders, *Jour. Geophys. Res.*, **72**:5705–5715.

Buckingham, W. F., and S. E. Sommer, 1983. Mineralogical characterization of rock surfaces formed by hydrothermal alteration and weathering - applications to remote sensing, *Economic Geology*, **78**(4):664–674.

TABLE 4. SUMMARY OF FACTORS CONTRIBUTING TO SKARN / HORNFELS DISCRIMINATION BY (0.717 TO 0.873-μM) DIFFERENCE IMAGE.

Possible source of discrimination	Theorized effect on spectra	Why considered in this study	Actual effect on spectra
Iron content	Minerals with greater Fe-content may show stronger Fe-absorption	Skarn garnets are considerably more iron-rich than hornfels	Some effect; garnets show increase in depth of Fe^{3+} minimum at 0.873 μm
Grain size	Coarser grain size results in deeper absorption minima	Skarn is generally coarser-grained than hornfels	Probably contributes, but by itself is only a minor factor
Weathering styles	Different weathering styles or products may result in different spectra	Skarn and hornfels contain different grain size and quantities of garnet & pyroxene	Major factor in discrimination; greater quantity of fine-grained pyroxenes in hornfels weather easily and reduce brightness in channel **5** relative to channel **8**.

Clark, R. N., and T. L. Roush, 1984. Reflectance spectroscopy: quantitative analysis techniques for remote sensing application, *Jour. Geophys. Res.*, **89**(B7):6329–6340.

Crowley, J. K., 1986. Visible and near-infrared spectra of carbonate rocks: reflectance variations related to petrographic texture and impurities, *Jour. Geophys. Res.*, **91**:5001–5012.

Dilles, J. H., 1987. Petrology of the Yerington batholith, Nevada: evidence for the evolution of porphyry copper ore fluids, *Economic Geology*, **82**:1750–1789.

Dilles, J. H., and M. T. Einaudi, 1992. Wall-rock alteration and hydrothermal flow paths around the Ann-Mason porphyry copper deposit, Nevada - a 6-km vertical reconstruction, *Economic Geology*, **87**:1963–2001.

Einaudi, M. T., 1977. Petrogenesis of the copper-bearing skarn at the Mason Valley Mine, Yerington district, Nevada, *Economic Geology*, **72**:769–795.

———, 1982. General features and origin of skarns associated with porphyry copper plutons, *Advances in the Geology of the Porphyry Copper Deposits: Southwestern North America*, (S. R. Titley, editor), University of Arizona Press, Tucson, pp. 185–210.

Einaudi, M. T., L. D. Meinert, and R. J. Newberry, 1981. Skarn deposits, *Economic Geology 75th Anniversary Volume* (B. J. Skinner, editor), Econ. Geol. Publishing Co., El Paso, Texas, pp. 317–391.

Green, A. A., and M. D. Craig, 1985. Analysis of aircraft spectrometer data with logarithmic residuals, *Proc. 1st Airborne Imaging Spectrometer Data Analysis Workshop*, 8-10 April, Jet Propulsion Laboratory, California Institute of Technology, Pasadena, California, pp 111–119.

Harris, N. B., 1979. *Skarn Formation near Ludwig, Yerington District, Nevada*, unpub. PhD dissertation, Stanford University. 172 p.

Harris, N. B., and M. T. Einaudi, 1982. Skarn deposits in the Yerington district, Nevada: metasomatic skarn evolution near Ludwig, *Economic Geology*, **77**:877–898.

Hunt, G. R., J. W. Salisbury, and C. L. Lenhoff, 1973. Visible and near-infrared spectra of minerals and rocks: VI. Additional silicates, *Modern Geology*, **4**:85–106.

King, T. V. V., and W. I. Ridley, 1987. Relation of the spectroscopic reflectance of olivine to mineral chemistry and some remote sensing implications, *Jour. Geophys. Res.*, **92**(B11):11,457–11,469.

Knopf, A., 1918. *Geology and Ore Deposits of the Yerington District, Nevada*, U.S.G.S. Professional Paper 114, 68 p.

Lyon, R. J. P., 1962. *Evaluation of Infrared Spectrophotometry for Compositional Analysis of Lunar and Planetary Soils*, Stanford Research Institute (under Contract No. NASr-49(04) NASA TN D-1871), 140 p.

———, 1964. *Evaluation of Infrared Spectrophotometry for Compositional Analysis of Lunar and Planetary Soils: Rough and Powdered Surfaces*, Stanford Research Institute (under Contract No. NASr-49(04) NASA CR-100), 167 p.

———, 1965. Analysis of rocks by spectral infrared emission (8 to 25 microns), *Economic Geology*, **60**:715–736.

Lyon, R. J. P., and A. A. Green, 1975. Reflectance and emittance of terrain in the mid-infrared (6-25 m) region, *Infrared and Raman Spectroscopy of Lunar and Terrestrial Minerals* (C. Karr, Jr., editor), Academic Press, New York, pp. 165–195

Lyon, R. J. P., and F. R. Honey, 1990. Direct mineral identification (DMI) with Geoscan MkII Advanced Multi-Spectral Scanner (AMSS), *Proc. Imaging Spectroscopy of the Terrestrial Environment*, 16-17 February, pp. 50–61.

Lyon, R. J. P., F. R. Honey, and G. I. Ballew, 1975. A comparison of observed and model predicted atmospheric perturbations on target radiances measured by ERTS: Part 1 - Observed data and analysis, *Proc. 6th Conference on Decision and Control and 14th Symposium on Adaptive Processes*, 10-12 December, Houston, Texas, pp. 244–249.

Moore, R. K., and W. B. White, 1972. Electronic spectra of transition metal ions in silicate garnets, *Canadian Mineralogist*, **11**:791–811.

Proffett, J. M., 1977. Cenozoic geology of the Yerington district, Nevada, and implications for the nature and origin of Basin and Range faulting, *G.S.A. Bulletin*, **88**:247–266.

Proffett, J. M., and J. H. Dilles, 1984. *Geologic Map of the Yerington District, Nevada*, Nevada Bureau of Mines and Geology Map 77, Reno, Nevada.

———, in press. Early Mesozoic sedimentary and volcanic rocks of the Yerington region, Nevada, and their regional context, *U.S. Geological Survey Centerpiece Project on Mesozoic Geology, Geophysics and Ore Deposits of Western Nevada*, U.S.G.S. Bulletin.

Roberts, D. A., Y. Yamaguchi, and R. J. P. Lyon, 1986. Comparison of various techniques for calibration of AIS data, *Proc. 2nd Airborne Imaging Spectrometer Data Analysis Workshop*, 6-8 May, Jet Propulsion Laboratory, California Institute of Technology, Pasadena, California, pp. 21–30.

Rubin, T. D., 1991. *Spectral Alteration Mapping with Ground Measurements and Remote Sensing at Yerington, Nevada*, unpub. PhD. dissertation, Stanford University, 182 p.

———, 1993. Spectral mapping with imaging spectrometers, *Photogrammetric Engineering & Remote Sensing*, **59**:215–220.

Salisbury, J. W., and G. R. Hunt, 1968. Martian surface materials - effect of particle size on spectral behavior, *Science*, **161**:365–366.

Salisbury, J. W., L. S. Walter, N. Vergo, and D. D'Aria, 1991. *Infrared (2.1-25 μm) Spectra of Minerals*, The Johns Hopkins University Press, Baltimore, 267 p.

Straub, D. W., R. G. Burns, and S. F. Pratt, 1991. Spectral signature of oxidized pyroxenes: implications to remote sensing of terrestrial planets, *Jour. Geophys. Res.*, **96**(E3):18,819–18,830.

Townsend, T. E., 1987. Discrimination of iron alteration minerals in visible and near-infrared reflectance data, *Jour. Geophys. Res.*, **92**(B2):1441–1454.

Windeler, D. S., 1992. *Spectral Mineral Mapping of Skarns and Hornfelses of the Yerington District, Nevada, Using Airborne Multispectral Data*, unpub. MS thesis, Stanford University, 207 p.

Windeler, D. S., and R. J. P. Lyon, 1991. Discriminating dolomitization of marble in the Ludwig skarn near Yerington, Nevada using high-resolution airborne infrared imagery, *Photogrammetric Engineering & Remote Sensing*, **87**(9):1171–1177.